

Origin of the absarokite–banakite association of the Damavand volcano (Iran): trace elements and Sr, Nd, Pb isotope constraints

J. M. Liotard · J. M. Dautria · D. Bosch ·
M. Condomines · H. Mehdizadeh · J.-F. Ritz

Received: 14 March 2006 / Accepted: 12 December 2006 / Published online: 23 January 2007
© Springer-Verlag 2007

Abstract The activity of the Damavand volcano (Central Alborz, northern Iran) began 1.8 Ma ago and continued up to 7 ka BP. Although the volcanic suite is clearly of shoshonitic affinity, only two petrographic types can be distinguished in the studied lavas: (1) weakly differentiated absarokites ($49 < \%SiO_2 < 51$), scattered around the volcano but with a regional extension, (2) highly differentiated banakites ($59 < \%SiO_2 < 63$), which form the bulk of the 4,000 m thick volcanic pile. All lavas are alkalic ($3.7 < \%K_2O < 5$), REE and LILE-rich (e.g., $85 < La < 148$ ppm; $9 < Th < 32$ ppm) and show highly fractionated REE patterns ($69 < La/Yb < 115$) and pronounced Nb–Ta negative anomalies. The absarokites are characterised by Sr (0.7045–0.7046) and Nd (0.51266–0.51269) isotope compositions close to the Bulk Earth values, and distinct from those of the banakites ($0.7047 < {}^{87}Sr/{}^{86}Sr < 0.7049$, $0.51258 < {}^{143}Nd/{}^{144}Nd < 0.51262$). The Pb isotope ratios are also slightly lower in the absarokites than in the banakites ($18.71 <$

${}^{206}Pb/{}^{204}Pb < 18.77$, $15.62 < {}^{207}Pb/{}^{204}Pb < 15.63$, $38.85 < {}^{208}Pb/{}^{204}Pb < 38.91$, and $18.77 < {}^{206}Pb/{}^{204}Pb < 18.84$, $15.62 < {}^{207}Pb/{}^{204}Pb < 15.64$, $38.94 < {}^{208}Pb/{}^{204}Pb < 39.06$, respectively). Overall, there is a clear tendency towards higher Sr, Pb and lower Nd isotope ratios with increasing degree of differentiation. This study suggests that the absarokites result from a low degree of partial melting (~5%) of a highly metasomatized mantle source, which inherited its characteristics from an old subduction setting. The initiation of volcanic activity 1.8 Ma ago results from variations in the lithospheric thermal regime, probably related to lithospheric delamination as proposed for Anatolia (Pearce et al. 1990). The banakites are mainly generated by extensive fractional crystallisation (~70%) of the absarokitic magma, with a limited amount (a few percents) of assimilation of an old crustal component, in the form of bulk assimilation or AFC processes, which both can explain the Sr, Nd and Pb isotope data.

Keywords Absarokite · Banakite · Trace elements · Sr · Nd · Pb isotopes · Damavand · Iran

J. M. Liotard (✉) · M. Condomines · J.-F. Ritz
Laboratoire de Dynamique de la Lithosphère, UMR 5573,
Université Montpellier 2 et CNRS, Place E. Bataillon,
34095 Montpellier Cedex 5, France
e-mail: liotard@dstu.univ-montp2.fr

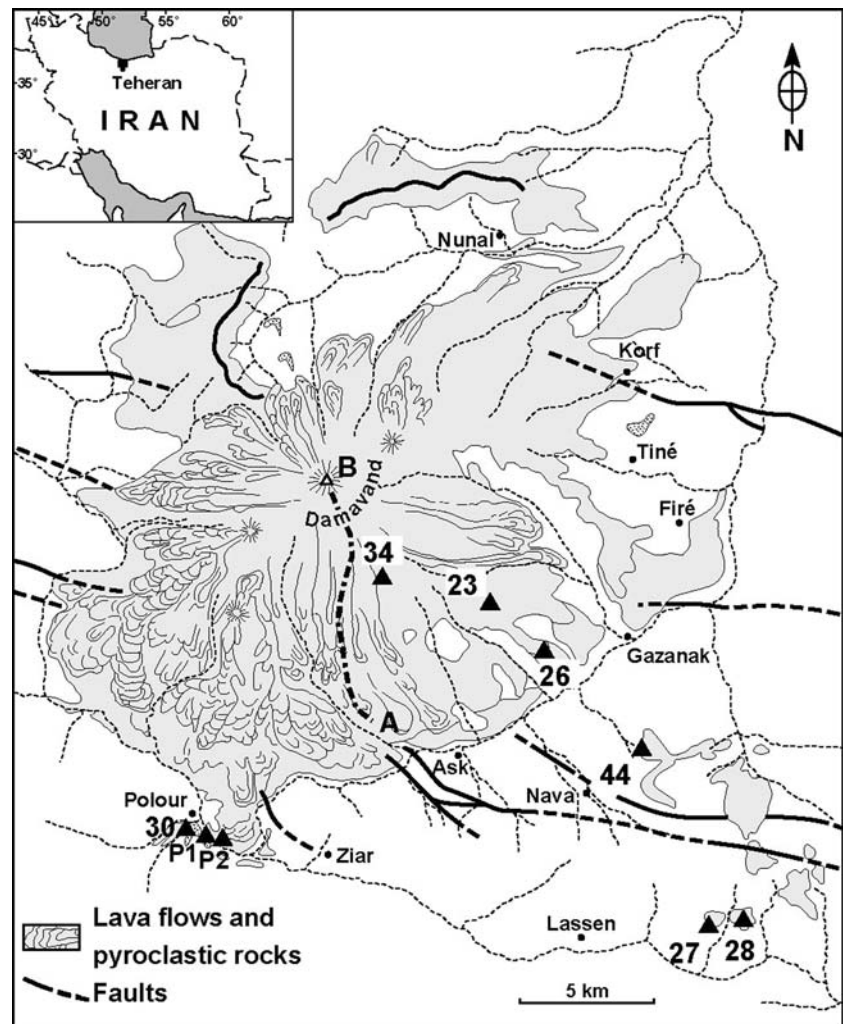
J. M. Dautria · D. Bosch
Laboratoire de Tectonophysique UMR 5568,
Université Montpellier 2 et CNRS, Place E. Bataillon,
34095 Montpellier Cedex 5, France

H. Mehdizadeh
Department of Geology, Shahrood University,
Shahrood, Iran

Introduction

Damavand is a young dormant strato-volcano (Fig. 1) located 50 km north of Tehran in the internal part of the Central Alborz, a polyorogenic mountain belt surrounding the South Caspian basin. The almost symmetric volcanic cone (400 km²) reaches an altitude of 5,670 m (4,000 m above the substratum). Its volume is estimated between 240 and 300 km³ and consists of pyroclastic breccias and lahars interbedded with thick

Fig. 1 Geological sketch map of Damavand volcano and location of samples DA P1, DA P2 and DH 23 to DH44. The references of the other samples (DA 2000–DA 5400) correspond to their height of collection along the path A–B to the summit



lava flows (Allenbach 1966; Brousse and Vaziri 1982; Davidson et al. 2004).

A detailed description of the geodynamic setting of the Alborz Mountains is given in a recent article of Davidson et al. (2004). The Damavand volcano is located in a peculiar zone where the trend of deformational structures rotates from NW–SE to SW–NE. According to the seismological data, the deformation in Alborz is partitioned along range-parallel thrusts and left-lateral strike-slip faults (Jackson et al. 2002; Allen et al. 2003). A recent GPS study accounts for a NS shortening of 5 ± 2 mm/year and a left-lateral shear of 4 ± 2 mm/year across the Alborz (Vernant et al. 2004). The left-lateral strike-slip movement may be concentrated on internal structure such as the Mosha fault along which a minimum Holocene left-lateral slip rate of 2 ± 0.1 mm/year has been estimated (Ritz et al. 2003a, b). The volcano outcrops 20 km northwards from the Mosha active fault and lays unconformably upon folds and thrusts affecting

sedimentary deposits ranging in age from Paleozoic to Cenozoic.

This volcano, although geographically isolated, belongs to the northern Cenozoic volcanic line, which stretches from Turkish Anatolia and Iranian Azerbaijan (with the Ararat, Sahand and Sabalan volcanoes) in the West to the Quchan volcanic area (Kopch Dag) in the East. Three magmatic series have been identified along this line: “calc-alkaline” in the Sahand and Ararat, “high-K calc-alkaline” in Sabalan (Innocenti et al. 1982) and “alkaline” in the Anatolian districts of Tendurek and Nemrut as also in the West Iranian district of Bijar and in the East Iranian district of Quchan (Berberian King 1981; Aftabi and Atapour 2000).

Due to their high SiO_2 and alkali contents, the Damavand lavas were previously considered as intermediate alkaline latites, trachyandesites and trachytes by Jérémme (1942), Bout and Derruau (1961) and more recently by Davidson et al. (2004). From major

element analyses, Brousse et al. (1977) and Brousse and Vaziri (1982) concluded that these lavas belong to a shoshonitic association. According to these authors, the Damavand volcano would be related to the subduction of an old oceanic crustal segment coming from the Zagros zone after the Miocene collision. Shoshonitic lavas are common in Iran with ages ranging from Eocene to Miocene (e.g., Aftabi and Atapour, 2000). The Damavand volcanics are the only one of Quaternary age. Therefore, understanding their origin and formation is a key to a better knowledge of the present-day geodynamic evolution of Northern Iran.

In spite of the lack of shoshonitic lava s.s., the shoshonitic character of the Damavand magmatic series was demonstrated in a previous paper of our group (Mehdizadeh et al. 2002). In the present contribution, sampling was extended by addition of five lavas collected between 2,000 m and the volcano summit and 3 from the peripheral volcanic area (Fig. 1). New K/Ar ages have been obtained for two samples and U-series disequilibria measured in two recent lava flows. Pb, Nd and Sr isotope compositions have been analysed in 12 lava samples. These new data are used to characterise the magma source and to propose a petrogenetic model for the volcano formation.

Analytical techniques

Major and trace element concentrations are given in Table 1. Major element concentrations were determined by XRF at the SARM (CRPG, Nancy) and trace elements concentrations by ICP-MS at the IS-TEEM (University of Montpellier II) following the analytical techniques outlined in Ionov et al. (1992). Sr, Nd and Pb isotopes were separated at the Laboratory of Tectonophysique (University of Montpellier II). Sr and Nd isotope compositions were measured on a Finnigan Mat mass spectrometer at the Paul Sabatier University (Toulouse). $^{87}\text{Sr}/^{86}\text{Sr}$ ratios of four NBS987 standards analysed during the course of this study yielded an average of 0.710245 ± 15 (2σ) ($n = 6$). $^{143}\text{Nd}/^{144}\text{Nd}$ ratios of “Rennes” standards yielded an average of 0.511987 ± 6 (2σ) ($n = 3$). Pb isotope compositions were determined by multicollector magnetic sector inductively coupled plasma-mass spectrometry using the VG model Plasma 54 in ENS (Lyon) (White et al. 2000). Samples were bracketed between NIST 981 standard splits and corrected according to values reported by Todt et al. (1995). K–Ar analyses have been performed at LSCE, CEA–CNRS, Gif sur Yvette. Age calculations are based on the decay and abundance constants of Steiger and Jäger

(1977): $\lambda\beta = 4.962 \times 10^{-10} \text{ a}^{-1}$; $\lambda_e = 0.581 \times 10^{-10} \text{ a}^{-1}$; $^{40}\text{K}/\text{K} = 1.167 \times 10^{-4} \text{ mol/mol}$. ^{238}U – ^{230}Th – ^{226}Ra – ^{210}Pb and ^{235}U – ^{231}Pa disequilibria were all measured through gamma spectrometry following the method described by Condomines et al. (1995). Due to the relatively high U and Th contents of the Damavand samples, it was also possible to measure (although with a lower precision) ^{230}Th , using the 67.7 keV gamma peak and ^{231}Pa (via the 236 keV peak of its daughter ^{227}Th).

Results

Age of eruptions

According to Allenbach (1966) and Davidson et al. (2004), Damavand volcano is constituted of two superimposed edifices. An “Old Damavand”, active between 1.8 and 0.8 Ma, subsequently eroded, is located slightly to the North and East of the present cone. A “Young Damavand”, active between 0.4 Ma and 7 ka, corresponds to the migration of activity centres towards the South and West. The “Old Damavand” activity was probably preceded and accompanied by regional basaltic emissions south and south-east of the volcano.

During this work, two flows have been dated by the K–Ar method (Table 1). The first one (DA2000), a differentiated lava collected near the village of Reynes at the foot of the volcano (point A, Fig. 1), belongs to the “Young Damavand”. It provides a K–Ar age of 410 ± 6 ka (Table 1). The second flow is a basalt (DH 44) outcropping near Nava (Fig. 1) and belongs to the regional basalt suite of the southeastern piedmont. It yields a K–Ar age of $1,480 \pm 20$ ka (Table 1). These two new ages are in good agreement with the recently published ages of Davidson et al. (2004).

In order to constrain the timing of the most recent activity of Damavand, we carried out a preliminary investigation of U-series disequilibria in two banakite samples (see Table 1). These samples come from two young lava flows: the first one (DA P1) outcrops at around 2,000 m asl in the Haraz River (SW Damavand), near Polour (Fig. 1). The second one (DA 4800), collected at 4,800 m asl, close to the summit of the volcano, belongs to the main volcanic pile (Fig. 1). The fact that ^{226}Ra and ^{230}Th are in radioactive equilibrium, whereas the ($^{230}\text{Th}/^{238}\text{U}$) and ($^{231}\text{Pa}/^{235}\text{U}$) ratios are both different from unity, suggests that the age of these banakites range between 8 and 160 ka (the latter corresponds to about five half-lives of ^{231}Pa). The age of these two banakites can be estimated at a few tens of

Table 1 Major, trace element, and Sr, Nd, Pb isotope compositions of the Damavand lavas (The analytical methods are given in Analytical techniques of the main text)

Sample	DH30*	DH44*	DH27*	DH28*	DH34*	DH26*	DA5400	DA P2	DA4800	DA4200	DH23*	DA2000
Rock type	Absarokite	Absarokite	Absarokite	Absarokite	Banakite							
SiO ₂	48.76	49.33	50.27	50.86	58.87	59.2	59.61	59.98	61.32	61.36	61.49	62.65
Al ₂ O ₃	14.91	15.73	15.74	15.47	16.01	15.89	16.44	16.09	16.41	16.03	15.93	16.16
Fe ₂ O ₃	8.63	8.58	7.57	7.52	5.79	5.54	4.19	4.84	4.9	4.71	4.92	4.67
MnO	0.12	0.11	0.1	0.1	0.07	0.06	< L.D.	0.05	0.05	0.05	0.06	0.06
MgO	8.39	7.25	6.66	6.66	3.31	2.82	1.27	2.61	2.46	2.22	2.24	1.99
CaO	7.93	7.37	7.68	7.55	4.82	4.67	3.38	4.74	3.84	3.76	3.96	3.83
Na ₂ O	3.79	4.55	4.53	5.14	4.83	4.85	4.55	5.04	4.86	4.73	4.84	4.69
K ₂ O	3.68	4.1	4	3.98	4.2	4.03	4.3	5.00	4.36	4.6	4.4	4.33
TiO ₂	1.78	1.76	1.38	1.38	1.11	1.01	0.92	0.94	0.94	0.88	0.89	0.86
P ₂ O ₅	1.16	1.1	1.24	1.24	0.65	0.55	0.36	0.64	0.48	0.47	0.5	0.41
PF	1.13	0.35	1.11	0.36	0.44	1.43	5.02	0.17	0.46	1.24	0.82	0.38
Total	100.28	100.23	100.28	100.26	100.1	100.05	100.04	100.10	100.08	100.05	100.05	100.02
K ₂ O/Na ₂ O	0.97	0.90	0.88	0.77	0.87	0.83	0.95	0.99	0.90	0.97	0.91	0.92
[Mg]	0.69	0.66	0.67	0.67	0.57	0.54	0.41	0.55	0.53	0.52	0.51	0.49
Ozn	0.00	0.00	0.00	0.00	3.44	5.04	9.14	2.05	7.08	7.64	7.73	10.09
Nen	8.79	12.94	10.86	13.51	0.00	0.00	0.00	0.00	0.00	0.00	0.00	0.00
Rb	41.8	66.2	50.8	53.4	124.5	107.8	124.6	127.3	131.4	142.6	140.7	137.5
Sr	2.210	2.000	2.200	2.850	1.590	1.150	1.340	1.580	1.370	1.310	1.250	1.110
Y	20.9	19.1	19.1	19.1	8.4	8.4	8.4	13.8	11.9	12.4	12.8	12.77
Zr	336	456	362	366	404	317	301	313	266	234	367	269
Nb	54.7	45.4	59.0	60.8	55.9	49.7	60.7	47.8	64.8	66.6	47.9	55.2
Cs	1.25	1.39	0.94	0.99	4.29	3.58	2.89	1.35	7.08	6.66	5.01	1.93
Ba	1.730	2.030	1.840	1.770	1.740	1.450	1.420	1.370	1.070	1.000	1.440	1.140
La	102.4	114.8	148.1	148.4	107.9	91.0	84.2	98.0	91.6	93.4	99.4	86.6
Ce	200.7	245.9	271.2	273.1	230.5	180.0	127.2	179.4	123.4	129.8	171.5	135.9
Pr	21.4	22.8	26.8	27.14	19.33	15.52	13.3	17.4	15.43	16.01	17.22	14.81
Nd	78.1	85.4	93.1	93.7	69.4	54.5	43.6	59.1	52.2	54.1	58.7	50.2
Sm	10.88	11.18	11.75	11.68	8.88	6.99	5.37	7.65	6.96	7.09	7.46	6.73
Eu	3.17	3.31	3.33	3.34	2.43	1.90	1.63	2.05	2.01	1.90	1.97	1.79
Gd	7.24	7.11	7.21	7.2	5.65	4.31	3.33	4.73	4.83	4.74	4.57	4.51
Tb	0.88	0.86	0.83	0.84	0.72	0.56	0.37	0.56	0.53	0.53	0.54	0.52
Dy	4.53	4.13	4.16	4.18	3.28	2.65	1.90	2.94	2.73	2.75	2.70	2.82
Ho	0.76	0.77	0.67	0.68	0.62	0.49	0.31	0.49	0.46	0.47	0.47	0.47
Er	1.96	1.88	1.72	1.71	1.60	1.23	0.84	1.27	1.18	1.24	1.23	1.28
Tm	0.25	0.25	0.21	0.22	0.21	0.16	0.11	0.17	0.16	0.17	0.16	0.17
Yb	1.49	1.51	1.29	1.36	1.29	1.03	0.77	1.06	1.04	1.09	1.02	1.06
Lu	0.24	0.23	0.19	0.2	0.21	0.15	0.12	0.16	0.16	0.17	0.16	0.16
Hf	7.33	9.18	7.57	7.68	8.42	6.43	7.47	7.61	7.42	6.05	8.21	7.32
Ta	3.14	2.77	2.81	3.03	3.99	3.47	3.80	3.12	3.75	4.01	3.45	3.74
Pb	11.6	14.3	14.9	15.0	20.6	18.0	12.5	16.9	9.4	11.8	19.1	23.6
Th	9.0	11.8	12.1	12.3	28.1	21.9	24.7	27.2	27.6	32.5	29.3	29.4
U	2.29	2.74	2.54	2.67	6.45	5.12	6.36	6.13	6.76	7.13	6.40	6.55

Table 1 continued

Sample	DH30*	DH44*	DH27*	DH28*	DH34*	DH26*	DA5400	DA P2	DA4800	DA4200	DH23*	DA2000
$^{208}\text{Pb}/^{204}\text{Pb}$ ($\pm 2\sigma$)	38.846 \pm 5	38.859 \pm 7	38.907 \pm 4	38.894 \pm 7	38.966 \pm 5	38.953 \pm 8	38.959 \pm 7	38.990 \pm 3	38.943 \pm 9	38.968 \pm 8	38.996 \pm 9	39.061 \pm 5
$^{207}\text{Pb}/^{204}\text{Pb}$ ($\pm 2\sigma$)	15.627 \pm 5	15.615 \pm 5	15.622 \pm 3	15.619 \pm 6	15.629 \pm 4	15.623 \pm 7	15.629 \pm 5	15.636 \pm 3	15.629 \pm 7	15.624 \pm 7	15.631 \pm 7	15.638 \pm 4
$^{206}\text{Pb}/^{204}\text{Pb}$ ($\pm 2\sigma$)	18.711 \pm 3	18.726 \pm 6	18.765 \pm 2	18.770 \pm 6	18.797 \pm 3	18.798 \pm 4	18.790 \pm 7	18.797 \pm 3	18.766 \pm 4	18.796 \pm 8	18.799 \pm 7	18.843 \pm 3
$^{143}\text{Nd}/^{144}\text{Nd}$ ($\pm 2\sigma$)	0.512688 \pm 7	0.512656 \pm 4	0.512675 \pm 6	0.512668 \pm 7	0.512606 \pm 5	0.512623 \pm 4	0.512590 \pm 4	0.512626 \pm 4	0.512600 \pm 5	0.512601 \pm 4	0.512591 \pm 4	0.512577 \pm 4
$^{87}\text{Sr}/^{86}\text{Sr}$ (2 σ)	0.704496 \pm 13	0.704466 \pm 14	0.704550 \pm 12	0.704531 \pm 11	0.704813 \pm 10	0.704698 \pm 15	0.704781 \pm 11	0.704892 \pm 7	0.704788 \pm 9	0.704815 \pm 8	0.704796 \pm 12	0.704839 \pm 14
K/Ar age (Ma)	1.48 \pm 0.02											
U-series results												
Sample	U (ppm)	Th (ppm)	^{226}Ra (dpm/g)	Th/U	$(^{230}\text{Th}/^{232}\text{Th})$	$(^{230}\text{Th}/^{238}\text{U})$	$(^{226}\text{Ra}/^{230}\text{Th})$	$(^{210}\text{Pb}/^{226}\text{Ra})$	$(^{231}\text{Pa}/^{235}\text{U})$			
DA P1	6.30 \pm 9	25.7 \pm 1	5.52 \pm 3	4.08 \pm 6	0.88 \pm 7	1.18 \pm 9	1.00 \pm 8	0.987 \pm 13	1.49 \pm 8			
DA 4800	6.96 \pm 9	28.8 \pm 1	5.96 \pm 3	4.13 \pm 6	0.85 \pm 6	1.16 \pm 8	1.00 \pm 7	1.001 \pm 12	1.42 \pm 7			

Ozn, Nen: respectively quartz or nepheline normative content; [Mg]: Mg/Mg + Fe²⁺. *Major and trace elements from Mehdizadeh et al. (2002). U-series results are also reported for two young Damavand lavas. Reported errors (on the last significant digit) are 1 σ errors derived from counting statistics on samples and standard

ka, given that the ($^{231}\text{Pa}/^{235}\text{U}$) ratio is still rather high. It is in agreement with previously published ages for the young Damavand (Davidson et al. 2004).

Petrographic characteristics

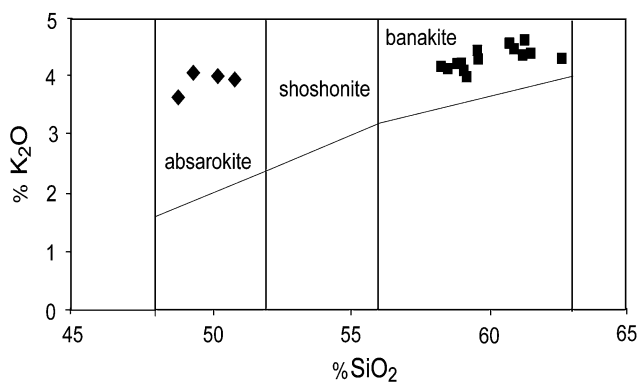
Major element analyses of mineral phases are given in Table 2. Absarokites appear as dark basalts, weakly porphyric (<10%) with phenocrysts of augite (Ca₄₇Mg₄₂Fe₁₁) and olivine (Fo₈₆). The groundmass, sometimes of fluidal texture, shows the same mineralogical assemblage but with additional plagioclase microliths and Ti-magnetite laths. Interstitial sanidine has been identified in some samples. Banakites are highly porphyric (30%) and resemble greyish andesites or dacites. The phenocryst assemblage contains plagioclase (An₃₂Ab₅₉Or₉), clinopyroxene (Ca₄₅Mg₄₂Fe₁₃), biotite (Mg/Fe = 0.62), olivine, magnetite (%TiO₂ = 6), ilmenite (%TiO₂ = 44) and apatite. The biotite phenocrysts always show figures of opaque mineral replacement in the outer zone. Some crystals have been completely pseudomorphosed. The plagioclase phenocrysts are strongly resorbed, showing marginal and internal melting evidences with sieve textures in some grains. Kaersutitic amphibole and orthopyroxene occur as microphenocrysts in several samples. Large apatite crystals (up to 2 \times 0.6 mm) are numerous and have a high LREE content (i.e., La₂O₃ = 0.39%). Zircon inclusions occur in clinopyroxene phenocrysts. Aggregates (up to 5 mm diameter) of clinopyroxene, plagioclase, biotite and apatite have been observed in numerous banakites. This suggests that crystal extraction (or accumulation) is the dominant process of the magmatic evolution of this series. The groundmass is composed of the same mineral phases as phenocrysts except olivine and biotite, which are absent.

Major, trace elements and isotopes

The major element analyses of whole rocks are given in Table 1. These data demonstrate the shoshonitic affinity of the series (Fig. 2). The more primitive lavas (absarokite) have a Mg# ranging from 0.66 to 0.69 and a SiO₂% close to 50. The differentiated terms (banakites) have a Mg# value between 0.41 and 0.57 with SiO₂% ranging from 58.9 to 62.6. The Na₂O contents are high (3.79 < Na₂O_{absarokites} < 5.14, 4.55 < Na₂O_{banakites} < 5.04) and do not correlate with SiO₂ or MgO contents. The K₂O contents are high in the absarokites (3.68 < K₂O% < 4.10) and only slightly higher in the banakites (4.03 < K₂O% < 5.00). The K₂O/Na₂O ratios of all lavas are slightly lower than 1 (0.83–0.97), which precludes an ultra-potassic character

Table 2 Average major element compositions of the phenocrysts in the studied lavas

	Absarokite		Banakite							
	Cpx	Ol	Cpx	Opx	Pl	Bi	Amp	Ap	Ti-Mt	Ilm
N	5	6	10	2	16	11	2	4	9	2
Percentage										
SiO ₂	49.30	40.28	52.64	55.20	59.70	35.05	42.18	0.38	0.72	0.08
Al ₂ O ₃	4.09	0.03	1.29	1.54	24.98	13.34	10.94	0.02	1.93	0.09
FeO	6.57	12.76	7.57	12.32	0.37	16.17	11.15	0.26	80.32	47.64
MnO	0.14	0.44	0.35	0.35	0.00	0.11	0.16	0.08	0.34	0.94
MgO	14.66	46.09	14.96	28.78	0.01	14.94	13.74	0.14	1.47	4.21
CaO	22.64	0.19	22.12	1.50	6.50	0.04	11.28	53.96	0.16	0.03
Na ₂ O	0.51	0.02	0.58	0.04	6.62	0.77	2.78	0.21	0.08	0.01
K ₂ O	0.01	0.00	0.01	0.01	1.53	9.25	1.29	0.01	0.04	0.06
TiO ₂	1.45	0.02	0.35	0.25	0.05	6.38	4.65	0.01	6.30	43.81
P ₂ O ₅	0.04	0.10	0.04	0.00	0.03	0.02	0.00	42.70	0.09	0.00
Cr ₂ O ₃	0.27	0.01	0.10	0.07	0.01	0.01	0.05	0.00	0.23	0.06
Σ	99.67	99.94	100.01	100.06	99.81	96.08	98.22	97.76	91.66	96.94

**Fig. 2** K₂O versus SiO₂ diagram from Peccerillo and Taylor (1976). Data from Mehdizadeh et al. (2002) and this study

for this series. These ratios are not correlated with the SiO₂ content. Compared to the banakites (see Table 1), the absarokites are enriched in P₂O₅ (1.1 < P₂O₅% < 1.24).

All samples are highly enriched in incompatible elements (e.g., 9 < Th_{ppm} < 32.5; 85 < La_{ppm} < 148). The most incompatible elements display two contrasted behaviours: Rb and U are positively correlated with Th, that suggests a classical fractionation process; Ba and La show weakly negative correlations with Th, that would result from fractionation of accessory minerals with high partition coefficient values for LREE and Ba, such as apatite and K-feldspar. The Primitive Mantle-normalized incompatible element diagrams (Fig. 3a, b) show the enriched character of all lavas but with variable degree (from several times for HREE to more than hundred times for Rb, Ba, Th, U, Pb). The REE are strongly fractionated (69 < La/Yb < 115). Significant negative anomalies are observed in the absarokites for Nb, Ta, and Ti. The Nb concentrations

and the Nb/Ta ratios are heterogeneous as well in the absarokites (45.4 < Nb_{ppm} < 60.8, 16.4 < Nb/Ta < 21.0) as in the banakites (47.3 < Nb_{ppm} < 66.6, 13.9 < Nb/Ta < 17.3). Such Nb/Ta values have been yet established in subduction related magmas from island arcs and continental margins (Green 1995). Compared with the typical mantle value (Nb/Ta = 17.5±2.0), the higher Nb/Ta may would result from fractionation of titanate minerals (such as rutile), while the lower would indicate contamination by collision zone granites with 5 < Nb/Ta < 12 (Green, 1995). The incompatible element patterns of the absarokites are also characterized by positive anomalies for Ba, and, to a lesser extent, for La, Pb and Sr. Negative anomalies in Nb, Ta, and Ti are also present in the banakites, with a significant positive anomaly for Pb (Fig. 3b). These features compare well with the data of Davidson et al. (2004) (Fig. 3c). However, these authors argued that their lavas are devoid of significant Nb–Ta anomalies and consequently have an alkalic affinity. This discrepancy is related to the lack of Th and U data in the diagrams presented by Davidson et al. (2004). Although the Nb–Ta anomaly of the Damavand lavas [i.e. (Nb/Th)/(Nb/Th)_{PM} = 0.58 and (Ta/Th)/(Ta/Th)_{PM} = 0.54 for the absarokites] is less pronounced than in subduction-related calc-alkaline series (i.e., Davidson et al. 1990), it still remains significant. In any case, the incompatible element distributions of absarokites are quite different from OIB (Fig. 3a), which display positive Nb–Ta anomalies [(Nb/Th)/(Nb/Th)_{PM} = 1.44; (Ta/Th)/(Ta/Th)_{PM} = 1.40] (Sun and MacDonough 1989). Moreover, the banakites have incompatible element patterns distinct from the differentiated terms of continental alkaline series (i.e., Maza 1998, Fig. 3b).

On a regional scale, the comparison between the Damavand banakites and the Ararat calc-alkaline

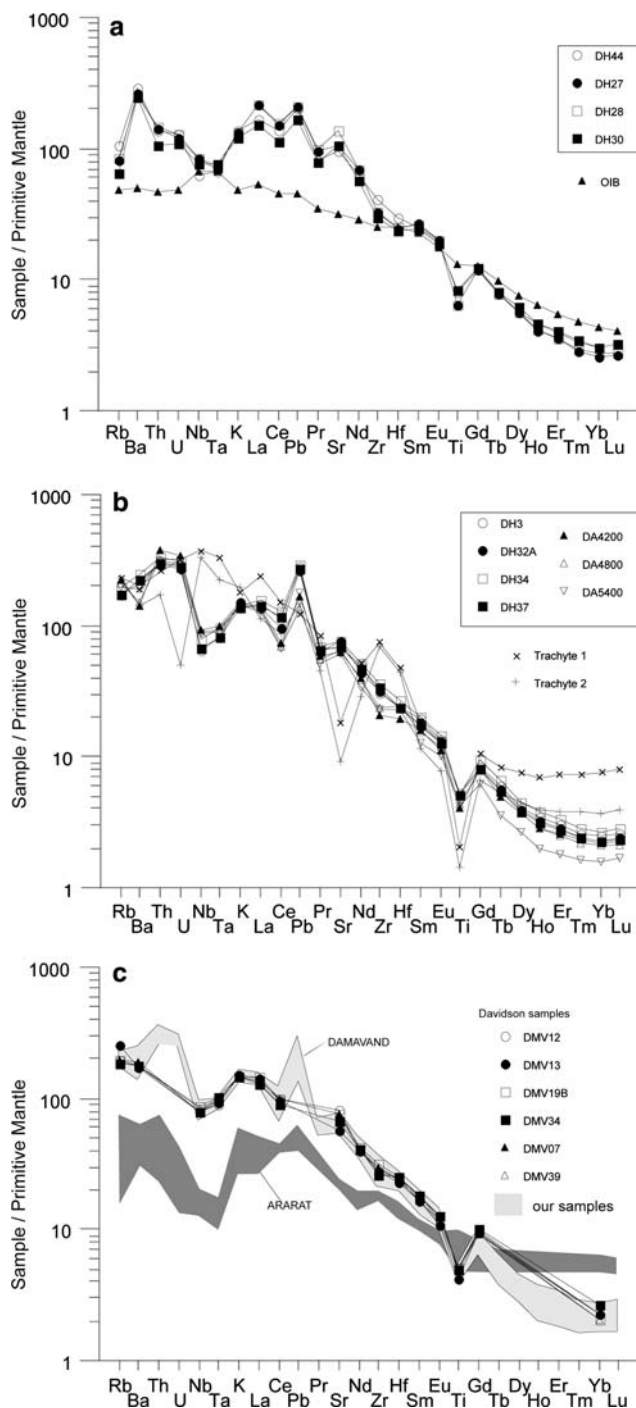


Fig. 3 Spidergrams of absarokite (a) and selected banakite (b) samples (data from Mehdizadeh et al. (2002) and this study). OIB sample, normalizing values of primitive mantle and incompatibility sequence are from Sun and MacDonough (1989); Tra1 and Tra2: trachytic samples from Ahaggar (Algeria) from Maza (1998), (c) Comparison between the Damavand banakite analyses of Davidson et al. (2004) and our data; Ararat lavas from Pearce et al. (1990)

lavas (Fig. 3c) shows significant differences which probably correspond to variations in the source composition (the Damavand banakites display a

strong enrichment in the most incompatible elements and a depletion in HREE). However the Nb/Ta anomalies observed both in the Ararat and Damavand lavas are quite similar.

The two petrographic groups display distinct isotope characteristics. The banakites show a restricted range of $^{87}\text{Sr}/^{86}\text{Sr}$ and $^{143}\text{Nd}/^{144}\text{Nd}$ ratios (0.70470–0.70489 and 0.51258–0.51263, respectively), distinct from the absarokites, which have lower $^{87}\text{Sr}/^{86}\text{Sr}$ ratios (0.70447–0.70455) and higher $^{143}\text{Nd}/^{144}\text{Nd}$ (0.51266–0.51269) isotopic compositions. In the Nd–Sr isotope diagram (Fig. 4a), the Damavand lavas plot close to the bulk earth composition and define a restricted domain located on the mantle array. Compared to other high-K series, they show similarities with Java and Aeolian island arc lavas (Edwards et al. 1991; De Astis et al. 2000; Ellam et al. 1989), but are clearly different from collision domains such as Tibet and Central Italy (Turner et al. 1996; Gasperini et al. 2002; Vollmer and Hawkesworth 1980; D’Antonio et al. 1996). Reported in the Pb–Pb isotope diagrams (Fig. 4b, c), the banakites ($18.766 < ^{206}\text{Pb}/^{204}\text{Pb} < 18.843$; $15.623 < ^{207}\text{Pb}/^{204}\text{Pb} < 15.638$; $38.943 < ^{208}\text{Pb}/^{204}\text{Pb} < 39.061$) and absarokites ($18.711 < ^{206}\text{Pb}/^{204}\text{Pb} < 18.770$; $15.615 < ^{207}\text{Pb}/^{204}\text{Pb} < 15.627$; $38.846 < ^{208}\text{Pb}/^{204}\text{Pb} < 38.907$) define two limited but distinct domains located outside the mantle array (see insets). They define a trend similar to that of the Andean lavas and are intermediate between the Java and Aeolian Island domains. The two banakite samples analysed for U-series disequilibria have the same Th/U ratio (4.1), and both display similar ^{230}Th – ^{238}U disequilibria, with a ($^{230}\text{Th}/^{238}\text{U}$) activity ratio of 1.17, and ($^{230}\text{Th}/^{232}\text{Th}$) ratio of 0.86. It is worth noting that these values are close to those of the present-day shoshonitic basalts erupted at Stromboli volcano in the Aeolian Islands [$\text{Th}/\text{U} = 3.83$; ($^{230}\text{Th}/^{238}\text{U}) = 1.135$; ($^{230}\text{Th}/^{232}\text{Th}) = 0.90$, Gauthier and Condomines 1999].

Discussion

Shoshonitic associations occur in various geological environments, often above subduction zones in intra-oceanic (Sun and Stern 2001, De Astis et al. 2000) or continental settings (Bourdon et al. 2003). However, they also occur in postcollisional geodynamic settings such as in Central Italy (Beccaluva et al. 1991; Gasperini et al. 2002), Tibet (Turner et al. 1996) and Anatolia (Innocenti et al. 1982). Whatever the setting, the geochemical characteristics of this magmatism (peculiarly the Nb, Ta and Ti negative anomalies) are classically considered as resulting from partial melting

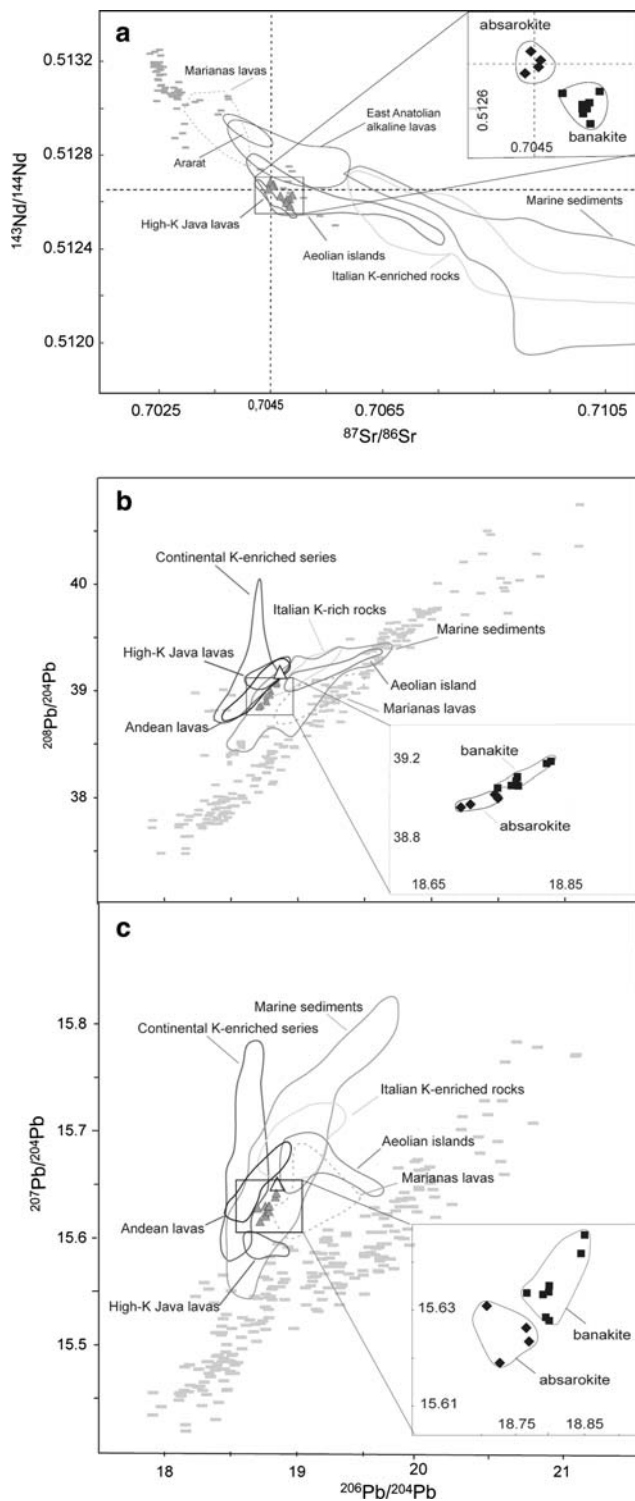


Fig. 4 Sr, Nd and Pb isotope diagrams for Damavand lavas. **a** Plot of $^{143}\text{Nd}/^{144}\text{Nd}$ versus $^{87}\text{Sr}/^{86}\text{Sr}$. Literature data sources are: Marine sediments (Ben Othman et al. 1989); Aeolian islands (De Astis et al. 2000; Ellam et al. 1989); High-K Java lavas (Edwards et al. 1991); Italian K-rich rocks (Gasperini et al. 2002; Vollmer et Hawkesworth, 1980; D'Antonio et al., 1996); Marianas lavas (Woodhead 1989; Sun and Stern 2001); Tibet (Turner et al. 1996); Andean lavas (Bourdon et al. 2003; Hickey et al. 1986); Ararat lavas (Gülen 1984). The mantle array is shown by grey sticks and comes from numerous literature data. Symbols: *black diamond* absarokite sample; *black square* banakite sample; **b** Plot of $^{208}\text{Pb}/^{204}\text{Pb}$ versus $^{206}\text{Pb}/^{204}\text{Pb}$ ratios. Same references and symbols as in Fig. 4a. The inset is the enlargement of the Damavand sample field. **c** Plot of $^{207}\text{Pb}/^{204}\text{Pb}$ versus $^{206}\text{Pb}/^{204}\text{Pb}$ ratios. Same symbols as in (a)

highly metasomatized mantle (e.g. Tatsumi and Koyaguchi 1989; Edwards et al. 1994; Turner et al. 1996). The high K_2O content of the Damavand absarokites (>4%), higher than the K_2O crustal average (Rudnick 1995), can only be explained in terms of a primary, source-related feature. This may reflect the presence of a potassic phase, most likely phlogopite, in the mantle source (Tatsumi and Koyaguchi 1989; Turner et al. 1996). This magmatic source is also characterized by low HREE abundances and high La/Yb ratios (69–115), that implies garnet as a residual phase. These very high values, much higher than OIB averages (La/Yb = 17, Sun and MacDonough 1989), suggest that the melting proportion of garnet in the absarokite source is lower than in the OIB source.

The K and trace element composition of the mantle source has been computed by assuming: (1) a metasomatized lherzolite composition for the source (Ol = 0.7, Opx = 0.19, Cpx = 0.05, Gt = 0.04, Phl = 0.02), (2) a melting degree f of 5%, (3) a non-modal melting model where the proportions p of liquid formed by melting of the above minerals are the following (Ol = 0, Opx = 0.01, Cpx = 0.58, Gt = 0.01, Phl = 0.40); note that the phlogopite is totally consumed in this process, and (4) mineral-melt partition coefficients for most trace elements from the GERM data base (Geochemical Earth Reference Model: <http://www.earthref.org>). The calculated source composition is reported in Fig. 5a. As expected, the source is enriched in incompatible elements, with enrichment factors (in the source compared to the primitive mantle) for strongly incompatible elements (Th, La) and K of 6.6, and a Nb negative anomaly. Only Ba has a significantly higher enrichment factor of around 13. Such features are commonly explained in terms of mantle source modifications by addition of slab-derived aqueous fluids leading to fluid-mobile LILE-enrichment and HFSE-depletion (e.g. Babaie et al. 2001).

of a highly metasomatized mantle associated with present or fossil slab sinking.

Origin of the absarokites

It is commonly admitted that absarokites result from low degree of partial melting ($2 < f < 5\%$) of a

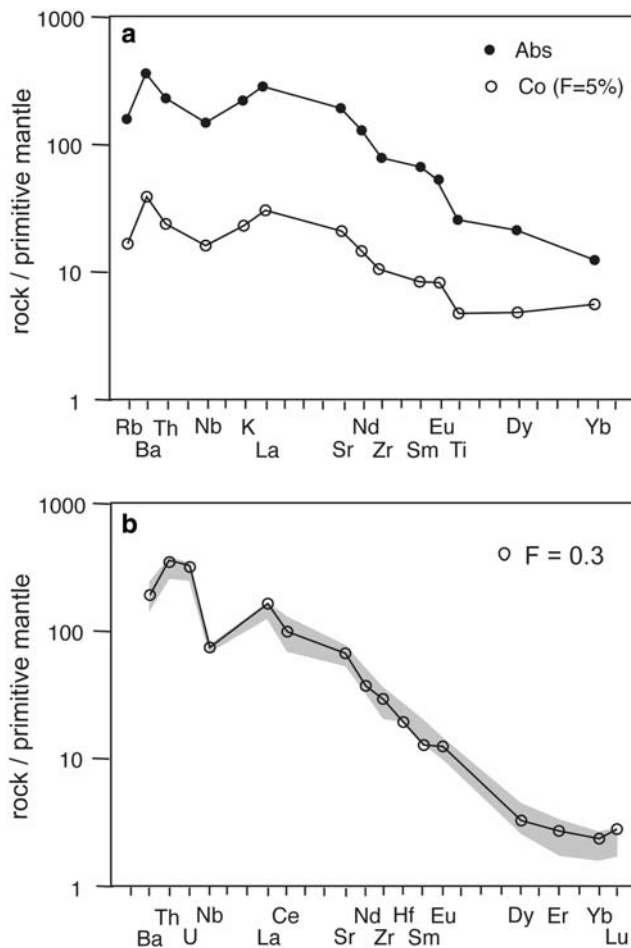


Fig. 5 **a** Average composition of absarokites, and calculated mantle source composition for a melting degree of 5% in a batch melting model (see text for detailed explanation). **b** Calculated composition of the residual melt after 70% crystallisation ($F = 0.3$) of an initial magma with the average absarokite composition. This curve is compared to the field defined by the banakites (in grey)

Thus, the Damavand lava genesis implies the presence of a mantle source enriched by fluids/melts derived from a subduction event. The age of this event is debatable: it could be recent and related to the initiation of subduction of the oceanic-like Caspian crust (Boulin 1991; Priestley et al. 1994); or it could be older than the late Neogene and related to the Zagros Belt formation (Brousse and Vaziri 1982; Aftabi and Ata-pour 2000). Unfortunately, the lithospheric structure beneath the Alborz Montains is poorly documented and the few available seismic data prevent any definitive conclusion about the presence of a slab and its depth (for references see Davidson et al. 2004). Nevertheless, the geochemical characteristics of the Damavand magmatism associated with the present post-collisional tectonic setting of Alborz rather suggest a situation similar to Tibet (Guo et al. 2005)

and Carpathians (Seghedi et al. 2001; Mahéo et al. 2002), where the presence of an ancient slab has been proposed. In the Damavand case, the paleotethyan subduction from southwest to northeast induced by the Zagros formation would be responsible for the metasomatism of the mantle source. The initiation of the volcanic activity (1.8 Ma) is not directly related to this subduction event. However, it suggests a recent change of the lithosphere thermal regime in this part of Alborz, probably in relation with the lithospheric delamination (e.g., Pearce et al. 1990).

Origin of the banakitic group

Major and trace element

Major element compositions suggest that the banakites could be derived from the absarokites through fractional crystallisation. The most incompatible elements (e.g., Th, U, Rb) strongly increase from the most primitive absarokite (DH 30) to the least evolved banakite (DH 26). If we apply the basic equation $C_1/C_0 = 1/F$ for Th, the observed variation (from 9.0 to 21.9 ppm) would imply a crystal fractionation amount of at least 60% without significant or only small variations of Na_2O , K_2O and Nb, Ta contents. The systematic discrepancy between the behaviour of the usually incompatible LREE (decreasing from the absarokites to banakites) and that of Th, U, Rb (increasing from the absarokites to banakites) suggests fractionation of mineral phases with contrasted partition coefficients for these two groups of elements (much higher values for the first one than for the second one). Apatite might be such a mineral. Its presence in the fractionating assemblage is corroborated by (1) the high P_2O_5 amount (>1%) measured in the absarokites compared to the lower values in the banakites (0.4–0.7%) (2) the occurrence of large apatite grains in the crystal aggregates observed in several banakites. The sharp decrease of HREE from absarokites to banakites suggests the additional fractionation of garnet and/or zircon. Garnet has not been identified in the present study, nor in the previous petrographic studies (Mehdizadeh et al. 2002). The Zr decrease from absarokites to banakites (from 457 in one absarokite to 234 ppm in one of the most differentiated banakites) and the occurrence of zircon inclusions in the minerals of aggregates favours the hypothesis of zircon fractionation (Table 3).

A detailed quantitative modelling of crystal fractionation is difficult, because of (1) the compositional variability in the analysed absarokites (probably due to variable melting degrees from 4 to 6%), (2) the fact

Table 3 Modelling crystal fractionation, mineral percentages in the cumulate, calculated through mass balance equations. *F* is the residual melt proportion

Percentage	Averaged Banakite	Averaged Absarokite	Recalculated Absarokite	Standard Deviation	<i>F</i> = 0.26
SiO ₂	61.34	50.33	50.41	-0.08	Segregate
Al ₂ O ₃	16.28	15.7	15.8	0.1	Ol = 6.9%
Fe ₂ O ₃	4.66	7.49	7.48	0.01	Cpx = 14.3%
MgO	2.55	7.75	7.68	0.07	Pl = 45.4%
CaO	4.29	7.35	7.21	0.14	Bi = 27.5%
Na ₂ O	4.9	4.57	3.7	0.87	Ap = 3.8%
K ₂ O	4.47	4.00	3.61	0.39	Ti-Mt = 2%
TiO ₂	0.96	1.6	1.8	-0.20	
P ₂ O ₅	0.54	1.2	1.38	-0.18	∑ r ² = 1.014
∑	99.99	99.99	99.07	0.91	SD = 0.507

that these latter might not strictly represent the parental absarokitic magma at the origin of banakites, and (3) the absence of intermediate products between absarokites and banakites. A rough calculation has nevertheless been made, using average compositions of both the absarokites and banakites. Major element modelling through classical least-square mass balance calculations shows that the average banakite composition could be derived from that of the average absarokitic magma after 74% fractionation of a cumulate composed of olivine (6.9%), clinopyroxene (14.3%), plagioclase (45.4%), biotite (27.5%), Ti-magnetite (2%) and apatite (3.8%)(Table 2). The main differences between the recalculated absarokite and the average starting absarokite composition concerns Na₂O and K₂O, and they suggest that the parental absarokitic magma was indeed poorer in Na and K than the analysed samples.

Of course, the mineral percentages calculated through this model refer to the bulk cumulate, and it is likely that crystal fractionation took place in several stages, each characterised by its own mineral assemblage. A knowledge of these various stages would be necessary for a precise modelling of trace element using a Rayleigh fractionation equation. It should be noted however that all the analysed trace elements have an incompatible behaviour ($D < 1$) in early crystallising mafic phases, like olivine, and clinopyroxene, so that their bulk partition coefficients will probably increase if successive stages of crystallisation are assumed, with an increasing proportion of plagioclase, biotite and accessory phases (Table 4). It can be shown that, in that case, the trace element contents of the differentiated magma calculated by using a single-stage model would represent maximum values. The trace element evolution has thus been modelled

Table 4 Distribution coefficients of trace elements used in Rayleigh fractionation modelling. Most partition coefficients are taken from the GERM database. *D* is the bulk partition coefficient for a segregate composed of 46% plagioclase, 27%

biotite, 14% clinopyroxene, 7% olivine, 4% apatite, 2% magnetite and 0.1% zircon (proportions deduced from major element modelling cf. Table 3)

	Distribution coefficients							<i>D</i>
	Cpx	Bi	Apat	Pl	Ol	Zr	Mt	
Ba	0.031	4	0.05	0.36	0.03	0.01	0.03	1.25
Th	0.019	0.16	2.76	0.004	0.014	22	0.05	0.18
U	-0	0.06	1.96	-0	-0	132	0.5	0.24
Nb	0.025	3.6	0.05	0.008	0.009	45	2.3	1.07
La	0.056	0.272	23	0.19	0.0067	5.25	0.22	1.10
Ce	0.092	0.318	28	0.11	0.006	3.49	0.12	1.27
Sr	0.25	0.672	2.4	2.4	0.053	-0	0.11	1.42
Nd	0.23	0.29	30	0.09	0.0059	3.8	0.25	1.36
Hf	0.014	0.2	0.03	0.36	0.0005	977	0.71	1.24
Sm	0.445	0.26	33	0.07	0.007	5.16	0.29	1.50
Eu	0.474	0.237	26	0.443	0.0074	2.39	0.22	1.38
Dy	0.582	-0.3	30	0.063	0.013	31.4	0.44	1.35
Er	0.583	-0.3	23	0.057	0.0256	64.6	0.24	1.10
Yb	0.542	0.44	20	0.056	0.0491	128	0.24	1.16
Lu	0.506	0.33	14	0.053	0.0454	196	0.32	0.95

through a single stage Rayleigh fractionation process, using the mineral proportions calculated from major elements. An amount of 0.1% of zircon has been added to take into account the decrease of Zr. Indeed, the maximum proportion of zircon in the cumulate can be calculated by assuming that zircon is the only Zr bearing phase. The Zr variation from the absarokite with the highest Zr content to the banakite with the lowest Zr content would require 0.12% of zircon in the cumulate (a similar calculation using the average Zr contents of absarokites and banakites would give 0.08% of zircon). The mineral/liquid partition coefficient values are taken from the GERM website database (<http://www.earthref.org>). The calculated trace element distribution of the melt after 70% crystal fractionation is reported in Fig. 5b. For almost all elements, the calculated maximum concentrations are in the range of the banakitic compositions or slightly above it (Fig. 5b).

Sr, Nd and Pb isotopes

The existence of significant differences in Sr, Nd, Pb isotope compositions between absarokites and banakites, and within the banakites cannot be explained by crystal fractionation alone. The tendency towards higher Sr, Pb and lower Nd isotope ratios with increasing differentiation suggest that the Damavand magmas might have assimilated a radiogenic component during their storage and crystallisation in the crust. We have thus tested an assimilation-fractional crystallisation model (AFC), involving a Precambrian granitic basement as contaminant. The parameters used in these calculations are given in the caption of Fig. 6. Although Precambrian terranes do outcrop in Central Alborz in the vicinity of the Damavand (Sahandi and Soheili 2005), their geochemical and isotope characteristics are unknown, so the values chosen for the crustal component are simply reasonable values for upper crust granitoids, and the model is only intended to test the AFC hypothesis.

It can be seen from Figs. 6a–d, where Sr, Nd and Pb isotope ratios are plotted versus Th contents (i.e., differentiation), that an AFC process can indeed explain the Damavand data. With the assumed parameters, and an R value of 10 ($R = M_c/M_a$ is the ratio: mass of cumulates/assimilated mass) the banakites would require f values between 0.4 and 0.3 ($f = M/M_0$ is the ratio: total mass of residual banakitic magma /initial mass of absarokitic magma). These values would correspond to a percentage of contamination $x = M_a/(M_0 + M_a)$ ($x = (1-f)/(R-f)$) of 6–7%. An alternative model is also illustrated in Fig. 6: it involves contami-

nation of the absarokitic magmas by a simple assimilation (binary mixing M) of a crustal component, and then crystallisation (CF) of this magma in an upper crustal magma chamber, where it differentiates into a banakitic magma. In this case, small percentages of contamination are still possible, but the high Sr, Nd and (to a lesser extent) Pb contents of the absarokitic magma require a crustal component with much higher Sr, Pb and lower Nd isotope ratios, compared to the AFC model. Such characteristics can be found in Archaean granitoids (e.g., Bickle et al. 1989). Whatever the genetic model, it is clear that such low percentages of assimilation would not affect major or trace element composition in a significant manner (especially if the uncertainties in partition coefficients of trace elements are taken into account). Thus, the proportions of crystallising minerals calculated above remain valid.

Conclusion

The Damavand volcano is essentially composed of K-rich differentiated lavas (banakites) belonging to the shoshonitic series. They were emitted between 1.8 Ma and 7 ka and were accompanied, during the first phase of activity, by a peripheral absarokitic volcanism. The two types of lavas are strongly LILE enriched and display Nb–Ta negative anomalies generally considered as geochemical indicators of subduction.

The Damavand absarokites are primitive magmas as suggested by their mineralogy, geochemistry and isotope ratios. Their trace element compositions suggest they result from a low degree of partial melting (~5%) of a garnet and phlogopite-rich lherzolite (with an isotope composition close to the Bulk Earth) metasomatized by slab-derived fluids and melts derived from an older subduction episode. The initiation of volcanic activity might result from variations in the lithospheric thermal regime related to lithospheric delamination as proposed for Anatolia (Pearce et al. 1990).

The banakites probably result from extensive fractionation ($F \sim 0.3$) of a mineral assemblage (Pl + Cpx + Biot + Ol + Ti-Mt + Ap + Zircon) corresponding to the observed phenocryst paragenesis. The presence of accessory minerals like apatite or zircon in the cumulates explain some of the peculiarities of the banakites (i.e., their lower REE and Zr contents compared to the absarokites). The Sr–Nd–Pb isotopic compositions of these lavas, slightly but significantly different from the absarokites, and the variations within the banakite group can be accounted for by a small percentage (<10%) of assimilation of a

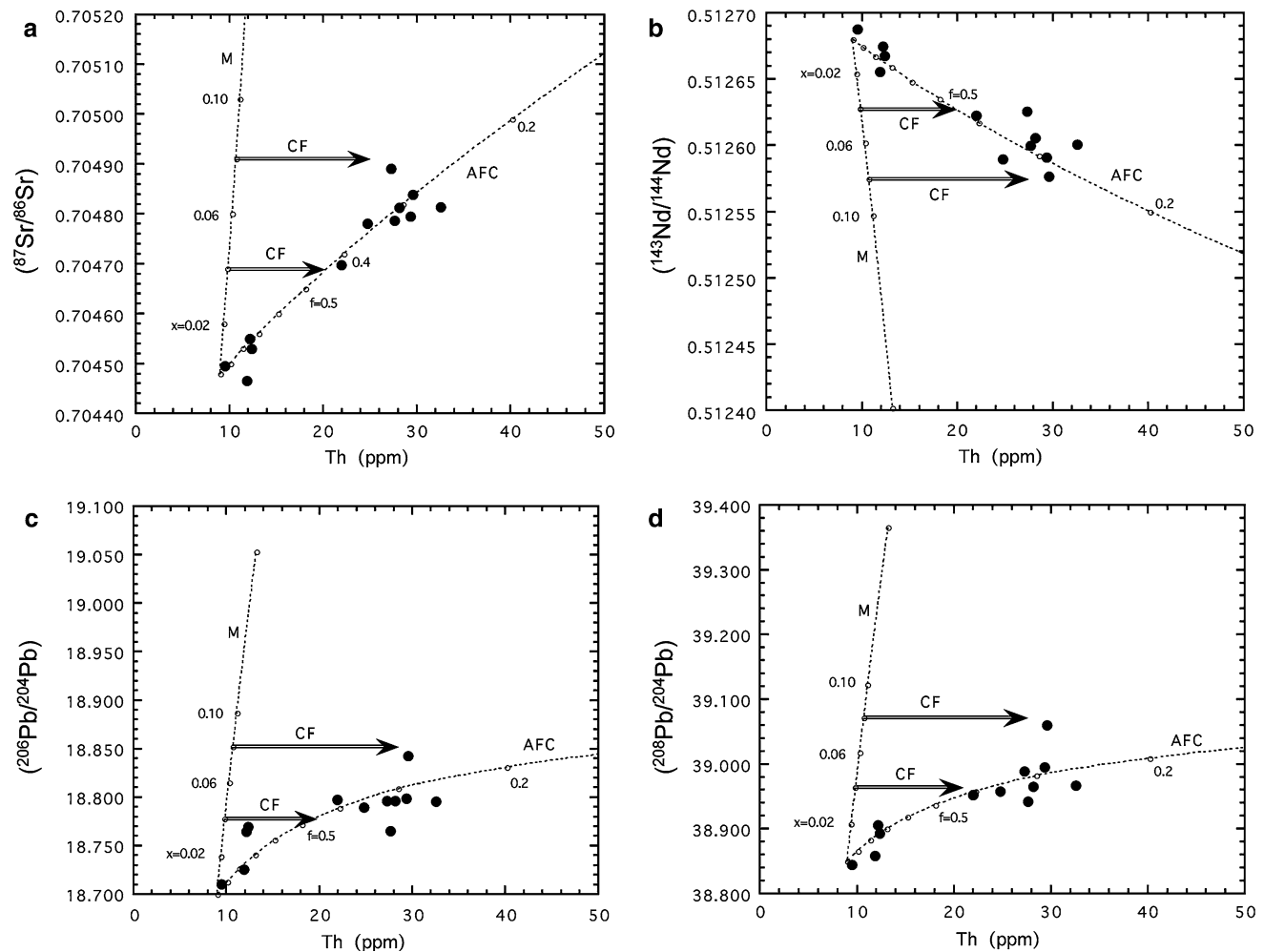


Fig. 6 Assimilation-fractional crystallisation (AFC) and assimilation (mixing M) followed by crystal fractionation (CF) models to explain Sr (a), Nd (b) and Pb (c, d) isotope ratios, plotted versus Th contents. For AFC models, the parameters used in the calculations are the following: Sr, Nd, Pb and Th contents of the assimilated crustal component are 350, 30, 20 and 30, respectively. The isotope compositions of this contaminant are: $(^{87}\text{Sr}/^{86}\text{Sr}) = 0.716$; $(^{143}\text{Nd}/^{144}\text{Nd}) = 0.5112$; $(^{206}\text{Pb}/^{204}\text{Pb}) = 19.4$; $(^{207}\text{Pb}/^{204}\text{Pb}) = 15.75$; $(^{208}\text{Pb}/^{204}\text{Pb}) = 39.7$. Bulk partition coefficients of 1.4, 1.4, 0.6 and 0.23 have been assumed for Sr, Nd, Pb and Th, respectively, and the ratio R (mass of cumulates/

assimilated mass) is equal to 10. The f values reported on the curves correspond to the ratio mass of residual magma/initial mass of magma. Note that our AFC models have been calculated to fit both Sr, Nd, Pb isotope ratios and contents of the analysed samples. For simple assimilation (M), the crustal component has the following characteristics: Sr, Nd, Pb and Th contents of 350, 50, 20 and 30 ppm, respectively. $(^{87}\text{Sr}/^{86}\text{Sr}) = 0.736$; $(^{143}\text{Nd}/^{144}\text{Nd}) = 0.5104$; $(^{206}\text{Pb}/^{204}\text{Pb}) = 19.9$; $(^{207}\text{Pb}/^{204}\text{Pb}) = 15.85$; $(^{208}\text{Pb}/^{204}\text{Pb}) = 40.6$. The x values reported on the curves indicate the proportions of assimilated component

crustal granitic component. Assimilation may be achieved either through a continuous AFC process or by simple assimilation in the anorogenic magma followed by crystal fractionation at an upper level.

Acknowledgments We thank Pierre Boivin (LMV, Université Blaise Pascal, Clermont-Ferrand) for generously providing his program for crystal fractionation calculations using major elements. We will also thank P. Brunet (LMTG, Toulouse University) who did the Sr isotope measurements and P. Telouk (ENS Lyon) for assistance with the P54 during running of Pb and Nd analyses.

References

- Aftabi A, Atapour H (2000) Regional aspects of shoshonitic volcanism in Iran. *Episodes* 23:119–125
- Allègre C J, Condomines M (1976) Fine chronology of volcanic processes using ^{238}U – ^{230}Th systematics. *Earth Planet Sci Lett* 28:395–406
- Allen MB, Ghassemi MR, Shahrabi M, Qorashi M (2003) Accommodation of the late Cenozoic oblique shortening in the Alborz range, northern Iran. *J Struct Geol* 25:659–672
- Allenbach P (1966) *Geologie und Petrographie des Damavand und seiner Umgebung (Zentral-Elbruz, Iran)*. Mitt Geol Inst ETH, Univ. Zürich 63, pp 114

- Babaie HA, Ghazi AM, Babaie A, La Tour TE, Hassanipak AA (2001) Geochemistry of arc volcanic rocks of the Zagros Crush Zone, Neyriz, Iran. *J Asian Earth Sci* 19:61–76
- Beccaluva L, Di Girolamo P, Serri G (1991) Petrogenesis and tectonic setting of the Roman volcanic province, Italy. *Lithos* 26:191–221
- Ben Othman D, White WM, Patchett J (1989) The geochemistry of marine sediments, island arc magma genesis, and crust-mantle recycling. *Earth Planet Sci Lett* 94:1–21
- Berberian M, King GC (1981) Towards a paleogeography and tectonic evolution of Iran. *Can J Earth Sci* 18:210–265
- Bickle MJ, Bettenay LF, Chapman HJ, Groves DI, McNaughton NJ, Campbell IH, de Laeter JR (1989) The age and origin of younger granitic plutons of the Shaw Batholith in the Archaean Pilbara Block, Western Australia. *Contrib Mineral Petrol* 101:361–376
- Boulin J (1991) Structures in Southwest Asia and evolution of the eastern Tethys. *Tectonophysics* 196:211–268
- Bourdon E, Eissen J-P, Gutscher M-A, Monzier M, Hall ML, Cotten J (2003) Magmatic response to early aseismic ridge subduction: the Ecuadorian margin case (South America). *Earth Planet Sci Lett* 205:123–138
- Bout P, Derruau M (1961) Le Demavend. C.N.R.S., Paris, Mém. et Doc. 8:9–102
- Brousse R, Vaziri HM (1982) L'association shoshonitique du Damavand (Iran). *Geologische Rundschau* 71(2):687–702
- Brousse R, Lefèvre C, Maury RC, Vaziri HM, Sobahni EA (1977) Le Damavand: un volcan shoshonitique de la plaque iranienne. *C R Acad Sci Paris Série D* 285:131–133
- Condomines M, Tanguy JC, Michaud V (1995) Magma dynamics at Mt Etna : constraints from U–Th–Ra–Pb radioactive disequilibria and Sr isotopes in historical lavas. *Earth Planet Sci Lett* 132:25–41
- D'Antonio M, Tilton GR, Civetta L (1996) Petrogenesis of Italian alkaline lavas deduced from Pb–Sr–Nd isotope relationships. In: Basu A, Hart S (eds) *Earth processes: reading the isotopic code*. AGU, Washington DC, pp 253–267
- Davidson JP, McMillan NJ, Moor bath S, Worner G, Harmon RS, Lopez-Escobar L (1990) The Nevados de Payachta volcanic region (18°S, 69°W, N. Chile): II. Evidence for widespread crustal involvement in Andean magmatism. *Contrib Mineral Petrol* 105:412–432
- Davidson J, Hassanzadeh J, Berzins R, Stockli DF, Bashukoo B, Turrin B, Pandamouz A (2004) The geology of Damavand volcano, Alborz Mountains, northern Iran. *GSA Bull* 116(1/2):16–29
- De Astis G, Peccerillo A, Kempton PD, La Volpe L, Wu TW (2000) Transition from calc-alkaline to potassium-rich magmatism in subduction environments: geochemical and Sr, Nd, Pb isotopic constraints from the island of Vulcano (Aeolian arc). *Contrib Mineral Petrol* 139:684–703
- Edwards CMH, Menzies MA, Thirlwall MF, Morros JD, Leeman WP, Harmon RS (1994) The transition to potassic alkaline volcanism in island arcs : the Ringgit–Beser complex, East Java, Indonesia. *J Petrol* 35:1557–1595
- Edwards C, Menzies MA, Thirlwall M (1991) Evidence from Muriah, Indonesia, for the interplay of supra-subduction zone and intraplate processes in the genesis of potassic alkaline magmas. *J Petrol* 32:555–592
- Ellam RM, Hawkesworth CJ, Menzies MA, Rogers NW (1989) The volcanism of Southern Italy: role of subduction and the relationship between potassic and sodic alkaline magmatism. *J Geophys Res* 94:4589–4601
- Gasparini D, Blichert-Toft J, Bosch D, Del Moro A, Macera P, Albarède F (2002) Upwelling of deep mantle through a plate window: Evidence from the geochemistry of Italian basaltic volcanics. *J Geophys Res* 107 B12:ECV7 1–19
- Gauthier PJ, Condomines M (1999) ^{210}Pb – ^{226}Ra radioactive disequilibria in recent lavas and radon degassing: inferences on the magma chamber dynamics at Stromboli and Merapi volcanoes. *Earth Planet Sci Lett* 172:111–126
- GERM (Geochemical Earth reference Model) home page. <http://www.earthref.org>
- Green T.H. (1995) Significance of Nb/Ta as an indicator of geochemical processes in the crust-mantle system. *Chem Geol* 120:347–359
- Gülen L (1984) Sr, Nd, Pb isotopes and trace element geochemistry of calc-alkaline volcanics of eastern Turkey. PhD, MIT, Cambridge, pp 232
- Guo Z, Hertogen J, Liu J, Pasteels P, Boven A, Punzalan L, He H, Luo X, Zhang W (2005) Potassic magmatism in western Sichuan and Yunnan provinces, SE Tibet, China. *J Petrol* 46:33–78
- Hickey RL, Frey FA, Gerlach DC, Lopez-Escobar L (1986) Multiple sources for basaltic arc rocks from the Southern Volcanic Zone of the Andes (34 degrees -41 degrees S); trace element and isotopic evidence for contributions from subducted oceanic crust, mantle, and continental crust. *J Geophys Res* 91:5963–5983
- Innocenti F, Manetti P, Mazzuoli R, Pasquaré G, Villari L (1982) Anatolia and north-western Iran. Andesites. Wiley, Chichester, pp 327–349
- Ionov DA, Savoyant L, Dupuy C (1992) Application of the ICP-MS technique to trace element analysis of peridotites and their minerals. *Geostandard Newsl* 16:311–315
- Jackson J, Priestley K, Allen M, Berberian M (2002) Active tectonics of South Caspian Basin. *Geophys J Int* 148:214–245
- Jérôme E (1942) Sur quelques roches du Demavend (Perse). *C R Acad Sci Paris* 215:163–165
- Mahéo G, Guillot S, Blichert-Toft J, Rolland Y, Pêcher A, (2002) A slab breakoff model for the Neogene thermal evolution of South Karakorum and South Tibet. *Earth Planet Sci Lett* 195:45–58
- Maza M (1998) Transition entre magmatisme tholéïitique et alcalin en contexte intracontinental; exemple du point chaud du Hoggar. Thesis, University of Montpellier II, pp 1–216
- Mehdizadeh H, Liotard JM, Dautria JM (2002) Geochemical characteristics of an intracontinental shoshonitic association : the example of the Damavand volcano, Iran. *CR Geosci* 334:111–117
- Pearce JA, Bender JF, De Long SE, Kidd WSF, Low PJ, Guner Y, Yilmaz Y, Moor bath S, Mitchell JG (1990) Genesis of collisional volcanism in eastern Anatolia, Turkey. *J Volcan Geoth Res* 44:189–229
- Peccerillo A, Taylor SR (1976) Geochemistry of Eocene Calc-alkaline volcanic rocks from Katsamonu Area, northern Turkey. *Contrib Mineral Petrol* 68:63–81
- Priestley K, Baker C, Jackson J (1994) Implications of earthquake focal mechanism data for the active tectonics of the south Caspian basin and surroundings regions. *Geophys J Int* 118:111–141
- Ritz J-F, Balescu S, Soleymani S, Abbassi M, Nazari H, Feghhi K, Shabanian E, Tabassi H, Farbod Y, Lamothe M, Michelot J-L, Massault M, Chery J, Vernant P (2003a) Geometry, Kinematics and Slip Rate Along the Masha Active Fault, Central Alborz, EGS-AGU-EUG Joint Assembly, Nice, France, 06–11 April 2003, Abstract EAE03-A-06057
- Ritz J-F, Balescu S, Soleymani S, Abbassi M, Nazari H, Feghhi K, Shabanian E, Tabassi H, Lamothe M, Michelot J-L,

- Massault M (2003b) Determining the Holocene slip rate along the Mosha Fault, Central Alborz. In: 4th international conference on seismology and earthquake engineering, 12–14 May 2003, Tehran
- Rudnick RL (1995) Nature and composition of the continental crust: a lower crustal perspective. *Rev Geophys* 33:267–309
- Sahandi M, Soheili M (2005) Geological Map of Iran at 1/1 000 000. Geol. Survey of Iran
- Seghedi I, Downes H, Pécskay Z, Thirwall M, Szakacs A, Prychodko M, Matthey D (2001) Magmagenesis in a subduction-related post-collisional volcanic arc segment: the Ukrainian Carpathians. *Lithos* 57:237–262
- Steiger RH, Jäger E (1977) Subcommittee on geochronology, convention on the use of decay constants in geo- and cosmochronology. *Earth Planet Sci Lett* 36:359–362
- Sun SS, McDonough WF (1989) Chemical and isotopic systematic of oceanic basalt: Implication for mantle composition and process. In: Saunders and Norry (eds). *Magmatism in Ocean Basins*. Blackwell, Geol Soc Spec. Publ, pp 313–346
- Sun C-H, Stern RJ (2001) Genesis of Mariana Shoshonites: contribution of the subduction component. *J Geophys Res* 106:589–608
- Tatsumi Y, Koyaguchi T (1989) An absarokite from a phlogopite lherzolite source. *Contrib Mineral Petrol* 102:34–40
- Todt W, Cliff RA, Hanser A, Hofmann AW (1995) Evaluation of a ^{202}Pb – ^{205}Pb double spike for high precision lead isotope analysis. In: Basu A, Hart S (eds) *Earth Processes: reading the isotopic code*. *Geophys Monogr, American Geophysical Union* 95:429–437
- Turner S, Arnaud N, Liu J, Hawkesworth C, Harris N, Kelley S, Van Calsteren P, Weng W (1996) Post-collision shoshonitic volcanism on the Tibetan plateau: implications for convective thinning of the lithosphere and the source of ocean island basalts. *J Petrol* 37:45–71
- Vernant P, Nilforoushan F, Chery J, Bayer R, Djamour Y, Masson F, Nankali H, Ritz J-F, Sedighi M, Tavakoli F (2004) Deciphering oblique shortening of Central Alborz in Iran using geodetic data. *Earth Planet Sci Lett* 223:177–185
- Vollmer R, Hawkesworth CJ (1980) Lead isotopic composition of the potassic rocks from Roccamonfina (South Italy). *Earth Planet Sci Lett* 47:91–101
- White WM, Albarède F, Telouk P (2000) High precision analysis of Pb isotope ratios by multi-collector ICP-MS. *Chem Geol* 167:257–270
- Woodhead JD (1989) Geochemistry of the Mariana Arc (western Pacific); source composition and processes. *Chem Geol* 76:1–24